PRE-NORMATIVE RESEARCH ON HYDROGEN RELEASES ASSESSMENT

D2.5

Calculation-based methods to quantify releases not covered by the experiments

AUTHORS

Name	Partner
Haris Nubli	SURREY
Jennifer Wen	SURREY
Jadwiga Holewa-Rataj	INIG
Mateusz Rataj	INIG
Tomasz Kuchta	INIG

The NHyRA project has received funding from the Clean Hydrogen Partnership under Grant Agreement No 101137770. This Partnership receives support from the European Union's Horizon Europe Research and Innovation program, Hydrogen Europe and Hydrogen Europe Research.

Co-funded by the European Union

TECHNICAL REFERENCES

Project Acronym	NHyRA
Project Title	PRE-NORMATIVE RESEARCH ON HYDROGEN RELEASES ASSESSMENT
Type	Research and Innovation Action (RIA)
Call Identifier	HORIZON-JTI-CLEANH2-2023-05-03
Topic	Pre-Normative Research on the determination of hydrogen releases from the hydrogen value chain
Project Coordinator	Matteo Robino
Project Duration	36 Months

Deliverable No.	2.5
Dissemination Level	PUBLIC
Work Package	WP2 - Methodology development for H2 releases quantification
Task	T 2.4 - Developing calculation-based methods to quantify the emissions sources not covered by the experiments
Lead beneficiary	SURREY
Contributing beneficiary(ies)	INIG, ENGIE, ENAGAS, BH
Due date of deliverable	30/06/25
Actual submission date	29/08/25

VERSIONS

Revision Version	Date	Changes	Changes made by Partner
0.1	June 2025	First release	SURREY INIG
0.2	July 2025	Reviews	WP2 partners
0.3	July 2025	Finalisation	SURREY

TABLE OF CONTENT

LIST OF FIGURES

LIST OF TABLES

EXECUTIVE SUMMARY

This report proposes methods for estimating hydrogen emissions from sources that are not cost effective by direct measurements. Thus, engineering calculations would be beneficial and effective for estimating several types of emissions which are developed in this task.

With hydrogen gaining prominence as a clean energy carrier, particularly in industrial and transport sectors, understanding and quantifying its potential environmental impacts is essential. The report categorises emission sources into fugitive emissions (e.g., pipe leaks), vented emissions (e.g., tank venting and purging), accidental releases occurring beyond normal operating conditions, and emissions from incomplete combustion.

To estimate emissions, a combination of empirical correlations and computational fluid dynamics (CFD) models is employed. These methods enable the calculation of hydrogen mass flow rates and total emissions by incorporating factors such as pressure, temperature, leak dimensions, and operating frequency. Equations were adapted from an existing method for methane emission quantification frameworks and validated using test data from related gases like CO_2, helium, and methane due to the limited availability of hydrogen-specific data. Validation against test data from past studies [1,2] showed good agreement, with discrepancies typically under 20%, confirming the suitability of the proposed methods.

An in-house software tool was developed using Python, featuring a graphical user interface (GUI) for user-friendly emissions calculator. The tool supports calculations for key emission scenarios—pipe joints and tank venting—and includes dynamic visualisations such as pressure drop and mass flow rate curves.

Furthermore, the current approach is constrained by data limitations, particularly regarding emission frequencies and failure rates specific to hydrogen systems. The report recommends further experimental work, field surveys, and database expansion to refine emission factors and improve quantification accuracy.

Overall, the methodologies and tools developed in this study provide a practical and validated foundation for assessing hydrogen emissions, helping to inform safety, regulatory compliance, and environmental impact assessments in the growing hydrogen economy.

1. INTRODUCTION

Global energy demand is increasing at an annual rate of approximately 1.2%, with fossil fuels such as petrol and diesel remaining the primary energy sources due to their reliability [3]. However, these fuels are major contributors to carbon dioxide (CO_2) emissions, which are projected to rise by 30% between 2005 and 2030 [3]. The international shipping industry alone accounted for around 2.7% of global greenhouse gas (GHG) emissions in 2007 [4]. In addition to CO_2, conventional fuel usage also leads to growing emissions of sulphur oxides (SO_x), nitrogen oxides (NO_x), and particulate matter (PM) [5,6]. As an initial response, the International Maritime Organization (IMO) established Emission Control Areas (ECAs) under Annex VI of the MARPOL Protocol, aiming to limit GHG emissions. These ECAs are currently enforced in regions such as North America and Europe [7].

To lessen reliance on fossil fuels, hydrogen is emerging as a promising zero-emission alternative. According to Det Norske Veritas (DNV), hydrogen fuel is expected to make up 4% of the maritime fuel mix by 2050, supporting the IMO's goal of achieving net-zero emissions in the sector [8]. It is hoped that hydrogen will become a widely adopted substitute for fossil fuels in the future energy landscape.

Recently, nearly all the world's annual hydrogen production—approximately 90 million tonnes per year—is used for non-energy purposes, according to DNV's hydrogen forecast to 2050 [9]. These applications primarily include desulphurisation of refined petroleum products, heavy oil upgrading in refineries, ammonia and methanol production, and hydrogen use in the direct reduction of iron for steelmaking [9]. However, DNV forecasts that hydrogen demand for household heating—mainly as a blend with natural gas—will increase to around 2 million tonnes per year by 2030 [9]. By 2050, demand for pure hydrogen as an energy source is expected to rise significantly, reaching approximately 12 million tonnes per year [9].

As a result of this growing demand, DNV projects that the average price of hydrogen will be cut in half by 2030 compared to 2020. This price reduction is expected to drive broader adoption of hydrogen for industrial heating, followed by increased use in household heating and transportation sectors [9]. By 2040, hydrogen prices are projected to fall within the range of USD 1–2 per kilogram. Hydrogen use in fuel-cell vehicles—particularly for long-distance heavy transport—is expected to expand, along with the adoption of ammonia as a marine fuel [9].

Despite offering a cleaner energy alternative—producing only water vapour during combustion—hydrogen gas consumes hydroxyl radicals (OH) and emits atomic hydrogen (H) during the initiation and propagation steps of the reaction. According to Ocko et al. (2022), this process may disrupt both the

troposphere and stratosphere [10]. The use of hydrogen as a fuel, particularly through combustion, reduces the availability of OH in the atmosphere [10,11]. Since OH is the primary sink for methane (CH_4), a decrease in OH leads to a longer atmospheric lifetime of methane, thereby potentially enhancing its warming effect over time [10,11].

Additionally, the production of atomic hydrogen from hydrogen oxidation in the troposphere can contribute to the formation of tropospheric ozone (O_3), a greenhouse gas that could account for approximately 20% of the radiative forcing associated with hydrogen use [10,11]. Moreover, the increase in atmospheric water vapour—especially at higher altitudes—can lead to stratospheric cooling, as more energy is emitted into space. However, this overall process contributes to climate warming, because the Earth emits less energy back into space and retains more heat [10,11].

Hydrogen can be stored and transported in various forms—such as compressed gas, cryo-compressed gas, or liquid hydrogen—each of which requires specially designed storage tanks [12,13]. Modern composite materials enable storage at pressures up to 100 MPa, while liquefied hydrogen, maintained at -252°C, offers greater energy density for large-scale use. Proper insulation is critical to prevent heat from entering the system, as thermal ingress can cause hydrogen to evaporate, increase internal pressure, and lead to fugitive emissions over extended storage periods [14,15].

In addition, during transportation and storage, excess hydrogen boil-off gas (BOG) may need to be vented to relieve pressure and protect the structural integrity of the tank—particularly in systems without a reliquefication unit. During loading and unloading operations, purging is required to remove residual hydrogen gas from the system, an essential safety measure to reduce the risk of fire [15,16].

Given the potential atmospheric risks associated with hydrogen emissions, it is crucial to accurately estimate the amount of hydrogen released into the environment. While direct measurements using gas detectors may be necessary for precise quantification, such physical methods can be labour-intensive and expensive. Furthermore, several emission sources—such as incomplete combustion or accidental leaks—are difficult to measure directly. As a result, numerical approaches, including empirical correlations and CFD, offer alternative methods for estimating hydrogen emissions. This report presents several methodologies for quantifying hydrogen emissions from a range of sources.

2. METHODOLOGY

To quantify hydrogen emissions that are not cost effective by conducting direct measurement, it is essential to consider various emission sources. According to existing methodologies, these sources can be categorized based on their flow characteristics—namely fugitive and vented emissions. Additionally,

incomplete combustion should be included in the assessment, particularly as hydrogen becomes more commonly used as a heating fuel.

This section outlines the general framework for quantifying emissions, which involves two key components: emission factors and activity factors.

- **Emission factors** represent the amount of hydrogen released—either intentionally or unintentionally—into the atmosphere, typically expressed as a mass flow rate. The calculation of mass flow rate varies depending on the emission source and can be determined using empirical correlations or numerical methods such as CFD.
- **Activity factors** reflect the frequency and intensity of emissions, taking into account the number of emission sources (e.g., devices) and the duration of hydrogen release. While the definition of activity factors is generally consistent across emission types, accidental releases require special consideration. In such cases, estimating the release frequency is necessary, as the total number of operational incidents leading to hydrogen emissions cannot be quantified directly.

2.1. Emission Sources

Emissions sources (in general) are typically grouped into the following categories, as defined in work package (WP) 1, Task 1.2:

a. Fugitive emissions:
   - Leaks due to connections/loss of tightness from components such as pipework and flanges.
   - Emissions from gas released from underground pipeline and salt cavern storage.

b. Vented emissions:
   - Normal operations, such as venting, purging and regular emissions of devices
   - Accidental release excluding the normal operations.

c. Incomplete Combustion:
   - Unburnt hydrogen in exhaust gases from combustion devices and its combustion efficiency.

These emissions may spread across a wide area, such as through multiple small vents. Emissions from maintenance activities (i.e., venting) can lead to high mass emission rates over a short duration. Monitoring these emissions may necessitate using instruments and sensors capable of handling and measuring pure hydrogen concentrations. Emission types which are considered in this quantification are shown in Table 1.

Table 1. Methods used for estimating hydrogen emissions

Emission Type	Emission Source	Method	Remarks
Fugitive	Above ground pipe joints	Empirical	-
	Underground pipe joints	Empirical	Gas flow through soil medium
	Salt cavern storage	Empirical	Emission due to cavern leakage
Vented	Tank venting	Empirical	Pressure relief under hydrogen loading process
	Tank inerting and purging	Empirical	Normal operation before loading and unloading
Incomplete combustion	Flaring	CFD	Estimates unburnt hydrogen
Accidental	-	Empirical	

2.2. General Concept of Quantification

Quantification involves measuring the amount of gas emitted from leaks of various origins, estimating emissions from groups of assets, or calculating based on available data. This following approach is based on a framework initially developed for quantifying methane emissions into the atmosphere by MarcoGaz [16], which is applicable to the current study.

The total H_2 emissions is given by Equation (1) [16]:

$$E = \sum_{i}^{N} E_{H_2,i} = \sum_{i}^{N} \left(EF_{H_2,i} \times AF_i \right) \quad (1)$$

Where:

- E is the total emission (kg). It is intended to be used over a one-year period, typically expressed in kg/year.
- $E_{H2,i}$ is the H_2 emissions of the *i-th* source (kg).
- $EF_{H2,i}$ is the emission factor of the *i-th* source expressed as a mass flow rate in kg per time unit and per event (or equipment), or as a H_2 quantity in kg.
- AF_i is the activity factor typically expressed as a result of multiplying number N of events (or equipment) by duration of H_2 leakage, or as the number N of events.
- n id the number of all covered emission source.

The AF is calculated as per Equation (2):

$$AF_i = N_i \times t_i \quad (2)$$

Where:

- N is the number of "i" events or equipment. Depending on category of emission, they can be for example: length of pipeline, number of leaks, number of vents, number of incidents, number of start & stops, number of devices/components.
- t_i is duration of H_2 leakage due to "i" event (or equipment).

3. EMPIRICAL CORRELATION-BASED CALCULATION

3.1 Fugitive Emissions

3.1.1. Flange Joints

The calculation of this leakage category will be focused on the pipe joints such as flanges. Based on the generic equation mentioned in the preceding section, the total emissions in kilogram per year can be expressed as:

$$E = EF \times AF = m_{total} \times N_{leaks} = Q_m \times t \times N_{leaks} \quad (3)$$

Where m_{total} is the total hydrogen mass that is calculated in kg, Q_m denotes the mass flow rate of hydrogen in kg/s, t is the leak duration in seconds which, for example, activation time of the emergency shutdown system could be considered, and N_{leaks} is the number of the detected leakage per year.

This equation is applicable for estimating annual hydrogen emissions in kilograms. However, accurately determining the number of leak incidents per year is challenging. One way to address this is by surveying each flange joint within a facility and gather the leakage data. To quantify an indirect measurement of hydrogen emissions, incorporating a failure frequency could be beneficial. There is component failure frequencies issued by Sandia National Laboratories (SNL) which includes a limited number of equipment used by hydrogen pipeline system [17]. Due to the scarcity of failure frequency data for hydrogen, accurately estimating its annual emission is challenging. Therefore, new or adjusted database is required. Figure 1 exhibits the typical equipment and connection used in the pipeline system including the flange joints.

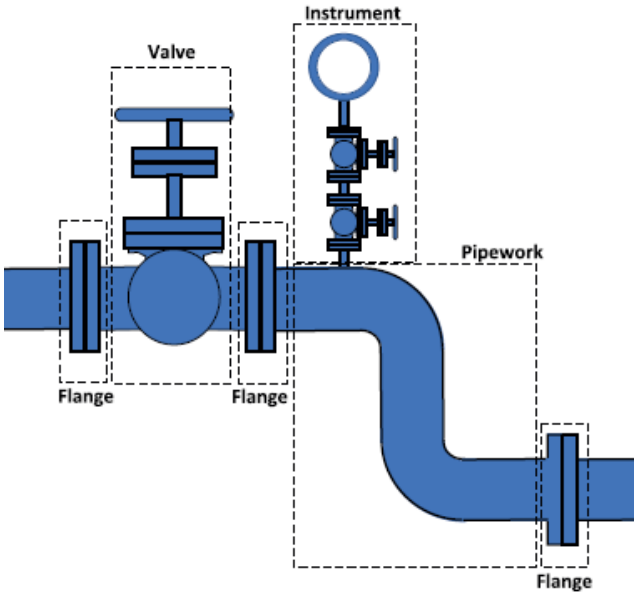

Figure 1. Typical equipment and joints in the pipeline system [18]

In order to include the failure frequency in the activity factor, the N_{leaks} can be considered as follows:

$$N_{leaks} = f_{leaks} \times n_{flanges} \tag{4}$$

where f_{leaks} denotes the frequency of flanges failure (/year), and $n_{flanges}$ denotes the number of installed flanges in a pipeline system. Subsequently, the tabulation of failure frequency with respect to leak category can be found in Appendix A.

Furthermore, the mass flow rate also can be estimated based on leak diameter by using a chocked-flow equation expressed as follows [19,20]:

$$Q_m = C_d A P_{abs} \sqrt{\frac{\gamma}{R_s T}} \left(\frac{2}{\gamma + 1} \right)^{\frac{\gamma+1}{2(\gamma-1)}} \tag{5}$$

where Q_m is the mass flow rate (kg/s), P_{abs} is the reservoir pressure (Pa), γ is heat capacity ratio, R_s is specific gas constant (J/(kg·K)), T is temperature (K) and d is hole diameter (m).

Meanwhile, for a subsonic flow, it can be expressed as follows [16]:

$$Q_m = C_d A \left(\frac{p_{atm}}{p_{abs}} \right)^{\frac{1}{\gamma}} \sqrt{2 \frac{\gamma}{\gamma - 1} p_{abs} \rho_{gas} \left(1 - \left(\frac{p_{atm}}{p_{abs}} \right)^{\frac{\gamma-1}{\gamma}} \right)} \tag{6}$$

where ρ_{gas} is fluid (gas) density (kg/m^3), C_d denotes discharge coefficient, p_{atm} and p_{abs} are atmospheric and absolute pressures, respectively. While A denotes the area of hole. To determine the gas density considering the pressure and temperature, the ideal gas law can be used as follows:

$$\rho_{gas} = \frac{p_{abs} \times M}{R \times T_{gas}} \tag{7}$$

where M denotes molar mass of gas which is 2.016×10^{-3} kg/mol for hydrogen, R denotes ideal gas constant which is 8.314 J/(K·mol), and T_{gas} is the gas temperature (K).

3.1.2. Underground Pipe

Estimating leakage behaviour and assessing the diffusion range outside the pipeline are crucial but challenging tasks because of the hydrogen mixture and soil conditions [21]. Measurement methods should involve direct survey techniques to gather data for future predictions or use a CFD approach that accounts for soil porosity. The basic Equation (1) remain applicable, though it requires modification of the emission factor (*EF*) while activity factor (*AF*) may account for the pipe failure frequency (i.e., weld joints).

$$E = EF \times AF = m_{total} \times N_{leaks} = Q_m \times t \times N_{leaks} \tag{8}$$

Due to the existence of soil above the leakage point, a parameter such as permeability should be considered. The simpler approach is by using Darcy's law for solving the emission factor. Furthermore, it only accounts for a single-phase flow [22]. Subsequently, the generalised form of Darcy's law is expressed as follows:

$$Q_V = \frac{kA}{\mu L}\Delta p = \frac{kA}{\mu L}\left(p_2 - p_1\right) \tag{9}$$

where Q_v denotes the volumetric flow rate (m^3/s), k denotes the permeability of soil (m^2) which is 0.1 to 1.0×10^{-4} m^2 for soil type like sand [23], μ is dynamic viscosity of the fluid (Pa·s), A denotes the cross-sectional area of leakage point (m^2), and P is pressure (Pa) which in this case is a gradient. In this case, L is employed as the distance over which the pressure drop is calculated (m), usually representing the length of the permeable media.

Furthermore, by adding the density of the fluid (ρ) in kg/m^3 in above equation, the mass flow rate (kg/s) can be obtained,

$$Q_m = \frac{kA\rho}{\mu L}\left(p_2 - p_1\right) \tag{10}$$

If temperature of gas and Forchheimer coefficient (β) are added, the basic equation of Darcy's law can be modified expressed as follows [16]:

$$Q_V = \frac{6\pi\mu r_{eq}^2}{\rho k \beta}\left[-1+\sqrt{1+\frac{k^2}{\mu^2}\frac{2\beta}{3r_{eq}RT_0}\left(p_2^2-p_1^2\right)}\right] \quad (11)$$

$$r_{eq} = \sqrt{\frac{A}{4\pi}} \quad (12)$$

where R denotes the specific gas constant (J/kg.K), T_0 is initial temperature of the gas (K), and r_{eq} denotes the equivalent radius of the leak (m). Since Q_V is a volumetric flow rate, it can be multiplied by gas density to obtain mass flow rate. Subsequently, to define the specific gas constant, c_v and c_p can be used which are the specific heat of constant volume and pressure, respectively in J/(kg.K). Thus, R is expressed as follows:

$$R = c_p - c_v \quad (13)$$

In this case, c_p and c_v of hydrogen are 14,290 and 10,160 J/(kg.K), respectively in normal temperature and pressure (NTP) [24]. Thus, R is 4,130 J/(kg.K).

Equation (11) can practically be applied by considering the properties of hydrogen gas and is based on the natural gas quantification method issued by MarcoGaz [16].

3.1.3. Salt Caverns Storage

Salt cavern hydrogen storage (SCHS) represents an essential advancement for large-scale hydrogen energy storage. However, hydrogen loss remains an issue in SCHS because of its high mobility and reactive chemistry. This loss not only raises expenses but also presents safety concerns. Identifying the primary factors that influence hydrogen loss in salt caverns is critical [25,26]. While hydrogen and natural gas exhibit distinct differences in their characteristics, they share similarities when it comes to leakage. Research has indicated that rock permeability is a crucial factor influencing gas leakage [25]. The leakage pathways for hydrogen in salt caverns consist of the rock salt, the interlayer, and the interface between the rock salt and the interlayer.

Nowadays, research on gas leakage in salt cavern gas storage primarily focuses on natural gas storage. According to Zhu et al., (2023), Equation (14) is applicable to estimate the hydrogen emissions from a salt cavern by considering the properties of hydrogen gas [25]. To investigate gas leakage rate (in kg/s) within salt cavern gas storage in salt domes, the following equation is formulated [25]:

$$Q_m = \left(p_o^2 - p_p^2\right) \frac{\pi kH}{\mu \ln\left(1+\sqrt{\frac{\pi kt}{\varphi \mu r^2}}\right)} \frac{273.15\rho_{STP}}{p_{atm} TZ} \quad (14)$$

$$Z = 1 + \alpha \frac{p_o}{T} \quad (15)$$

where p_o, p_p, and p_{atm} denote operating, pore, and atmospheric pressures (Pa), k is the permeability of rock salt (m^2), H denotes the height of salt cavern (m), μ denotes gas viscosity (Pa.s), ρ_{STP} is the density of gas at STP, T denotes the ambient temperature in the cavern, and Z denotes the compression coefficient. Furthermore, to calculate the compression coefficient, a fitting coefficient (α) is used which is 1.9155×10^{-6} for hydrogen gas [25,27]. Therefore, the emission and activity factors can be expressed as follows:

$$E = EF \times AF = Q_m \times t \times N_{saltdome} \quad (16)$$

where t is the storage duration (s) and $N_{saltdome}$ denotes the number of salt dome.

3.2 Vented Emissions

3.2.1 Venting

This category of emissions encompasses several activities, including the release of gases from pressurised tanks, tank trucks, and rail tank cars during filling or relief procedure due to an excess pressure [28].

For a hydrogen emission from venting process can be estimated as follows:

$$E = EF \times AF = m_{total} \times N_{vent} \quad (17)$$

where m_{total} denotes the total mass that emitted from the venting process in kilogram which can be measured by survey (direct measurement) or calculation using blow down equation, and N_{vent} is the number of venting processes. Since the mass flow rate varies during this process, a blowdown calculation must be considered due to the pressure drop presence. Thus, m_{total} can be expressed as:

$$m_{total} = \int_{t_1}^{t_2} \dot{m}(t)\, dt \quad (18)$$

where $\dot{m}$ is mass flow rate based on chocked-flow equation (Equation 5) in kg/s, and t denotes time during venting process in seconds. Furthermore, to account for the blowdown, the pressure term p_{bd} expressed as follows should be considered in Equation (5) to account pressure reduction [29]:

$$p_{bd} = p_0 \exp\left(-\frac{t}{\tau}\right) \quad (19)$$

where p_0 is initial or previous pressure of the tank with respect to the blow down time in Pascal, and τ denotes discharge time constant that can be described as follows [29]:

$$\tau = \frac{V_{tk}}{C_d A C_o \left(\frac{\gamma+1}{2}\right)^{\frac{\gamma+1}{2(\gamma-1)}}} \tag{20}$$

$$C_o = \left(\gamma \frac{RT_0}{M}\right)^{\frac{1}{2}} \tag{21}$$

where V_{tk} denotes the total volume of tank (m^3), C_d is a discharge coefficient, A denotes the area of vent outlet (m^2), γ is heat capacity ratio of the gas, C_o denotes the speed of sound at T_0 which is ambient temperature (in Kelvin), and M is molecular weight (mol).

3.2.2 Inerting and Purging

Nitrogen, an inert gas, is used to remove moisture and lower oxygen levels to below 4% in the storage tank and its connected piping. The inerting process involves repeated pressurisation and depressurisation cycles with nitrogen [30]. Moisture in the tanks or piping can result in the formation of hydrates—solid, ice-like structures that are difficult to dislodge. The presence of oxygen in the system could create an explosive atmosphere within the hydrogen transfer line, representing a significant safety risk that must be mitigated through inerting. Following this, the system is purged with hydrogen to eliminate any remaining nitrogen. In such cases, venting should be conducted via a gas control unit (GCU), oxidiser, or flare [30].

Since the focus is quantifying hydrogen, therefore, hydrogen fraction within the system must be considered. Thus, hydrogen emission from venting process can be estimated as follows:

$$E = EF \times AF = Q_m \times \omega_{H_2} \times t \times N_{purge} = m_{total} \times \omega_{H_2} \times N_{purge} \tag{22}$$

where ω_{H2} is the mass fraction of hydrogen in the system. Equations (5) or (18) can be utilised in this calculation to account for both constant-pressure releases and blowdown scenarios.

3.3 Accidental

The accidental release of gas, specifically hydrogen, could occur due to material failure of the equipment, including corrosion, malfunction at cryogenic temperatures, operational failure, human error leading to accidents, or rupture of equipment due to collisions or accidental loads [31,32].

Quantifying the loss of containment directly is challenging, as it is an irregular event. Therefore, utilising failure frequency is useful in understanding the probability of equipment failure that could lead to a gas

release. Since a gas release event can lead to multiple outcomes—such as gas dispersion (unignited release), fire, or explosion (ignited release)—the probability of ignition should be considered. To account for this, an event tree analysis can be used to determine the outcome frequency based on the branching paths. Typically, the analysis includes immediate and delayed ignition scenarios. Figure 2 shows a generic event tree for extremely flammable and pressurised liquefied gases.

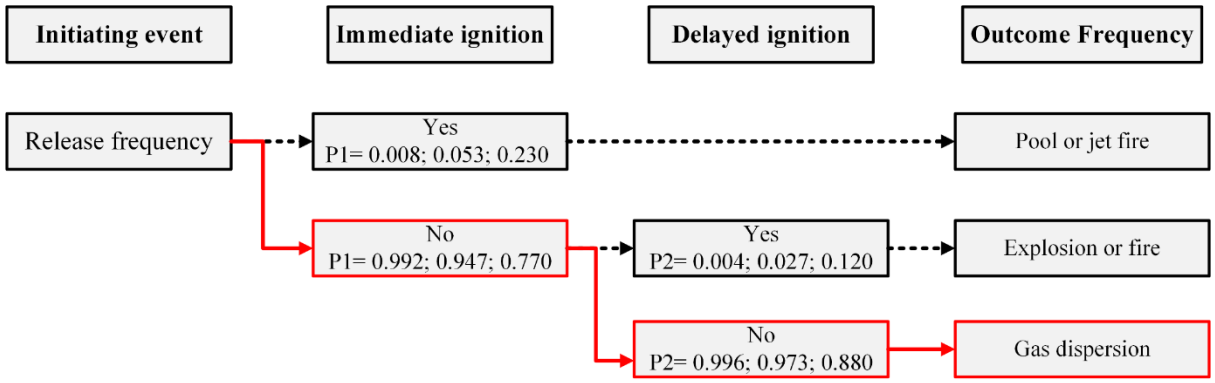

Figure 2. Event tree for continuous release of extremely flammable and pressurised liquefied gases [33]

According to Figure 2, there are two levels of ignition probability which encompasses immediate and delayed ignitions, P1 and P2, respectively. P1 and P2 values depend on the hydrogen release rate, given by HyRAM model [31], which are shown in Table 2. Since this study focuses on the quantification of hydrogen emissions, outcomes other than gas dispersion (red line) can be neglected. Therefore, the outcome frequency of gas dispersion ($f_{outcome}$) in /year, can be used as an activity factor. Furthermore, release duration (t) also should be included in the equation to estimate the total released mass. This parameter can be taken from the response time of emergency shutdown valve, otherwise, Equations (18) to (21) can be utilised for the case of tank leakage. These equations are expressed as follows:

$$E = EF_{acc} \times AF_{acc} = Q_m \times t \times N_{event} \tag{23}$$

$$N_{event} = f_{outcome} \times n_{equipment} \tag{24}$$

Table 2. Probability of ignition given by HyRAM model [31]

Hydrogen release rate (kg/s)	P1	P2
<0.125	0.008	0.004
0.125 – 6.25	0.053	0.027
>6.25	0.230	0.120

Furthermore, to account for release frequency, the failure frequency database in Appendix A can be utilised, which includes various equipment types and sizes. However, as concerned previously, the release frequency based on equipment failure frequency is limited to a small number due to data scarcity for hydrogen. New or adjusted frequency data need to be applied to improve the quality of the results.

3.4 Incomplete Combustion

The presence of unburned fuel can be understood through the combustion efficiency formula. During the combustion process, which occurs over a very short duration, fuel molecules may not always encounter oxygen molecules [34]. As a result, a small fraction of the fuel does not react and passes through to the exhaust channel. Combustion efficiency (η) accounts for the fraction of fuel that is burned. Equation (25) provides the basic equation for combustion efficiency, which incorporates density (ρ), mass fraction (Y), and cross-section of combustor (A). These components can be used to calculate the mass flow rate of fuel ($\dot{m}$) using averages over the respective combustor cross-section which expressed as follows [35,36]:

$$\eta_{unburned} = \frac{\int_A \rho \upsilon Y_{H_2} dA\,|_{reacting}}{\int_A \rho \upsilon Y_{H_2} dA\,|_{non-reacting}} = \frac{\dot{m}_{H_2}(x)}{\dot{m}_{H_2,injected}} \tag{25}$$

$$Q_m = \dot{m}_{H_2,injected}\,\eta_{unburned} \tag{26}$$

Therefore, Equation (26) can be employed to calculate the mass flow rate of the unburned fuel (Q_m) to fulfil the total emissions as follows:

$$E = EF_{device} \times AF_{device} = Q_m \times t \times N_{device} \tag{27}$$

where t denotes the duration of combustion in a device, and N_{device} is the number of devices.

The uncertainty of this method lies in the fact that combustion efficiency may vary over time due to changes in air and fuel temperatures or ignition timing in internal combustion engines. Therefore, the presented formula should only be applied under ideal conditions.

4. VALIDATION OF CORRELATION FORMULA

4.1 Validation of Gas Flow Through Orifice

An experimental data from Hammer et al. (2022) can be utilised to validate the mass flow equation [2]. This experiment provided various inputs, including temperature, initial pressure, and orifice diameter. The tests were conducted by utilising CO_2 gas considering the safety reason. Figure 3 shows the orifice geometry. Furthermore, Table 3 exhibits the specification of the tests and its measured mass flow rates.

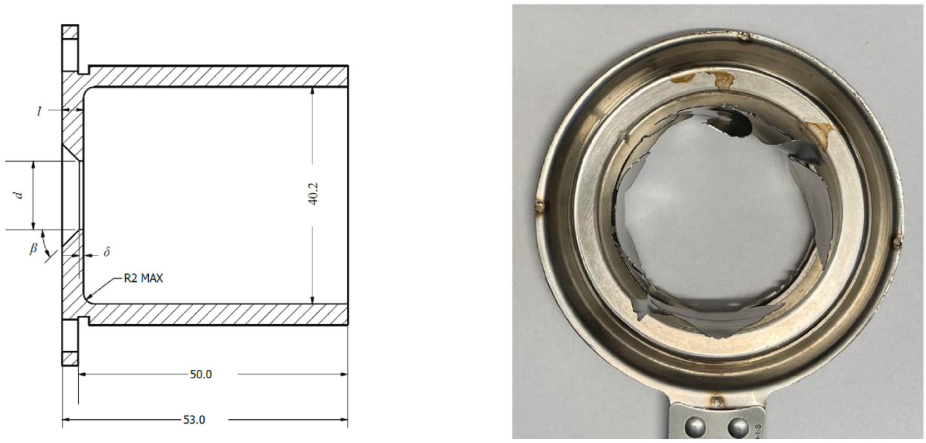

Figure 3. Geometry of the orifice used in the experiment [2]

Table 3. Test specification and the measured mass flow rates [2]

Test No.	T_0 (°C)	P_0 (MPa)	d (mm)	$\dot{m}$ (kg/s)
13	24.60	12.77	12.70	8.59
16	24.40	12.17	4.50	1.60
17	25.20	12.40	4.50	1.81
18	25.10	12.41	12.70	10.07
20	22.70	11.40	9.00	5.52
21	22.00	11.50	9.00	4.21

Since the gas flow through the orifice is in a choked condition, Equation (5) should be applicable for estimating the mass flow rate. Additionally, an extra calculation was performed, incorporating hydrogen gas properties while using the same variables listed in Table 3. The comparison is shown in Figure 4, and a tabulation of the plot is shown in Table 4. The R^2 score was used to compare the patterns of both data sets, showing a good agreement with a value of 0.996 out of 1.00. A higher R^2 value indicates a closer match in the patterns (i.e., slope) of the data. Subsequently, the experimental and predicted values were compared using the root mean squared error (RMSE). The results show a good agreement between the experimental and predicted mass flow rates using CO_2, with a discrepancy of 10.97 %. However, the

discrepancy between the CO_2 experiment and the predicted hydrogen flow rate is 48.01%, which is notably higher due to the differences in the properties of the gases, particularly the lower molar weight of hydrogen compared with CO_2.

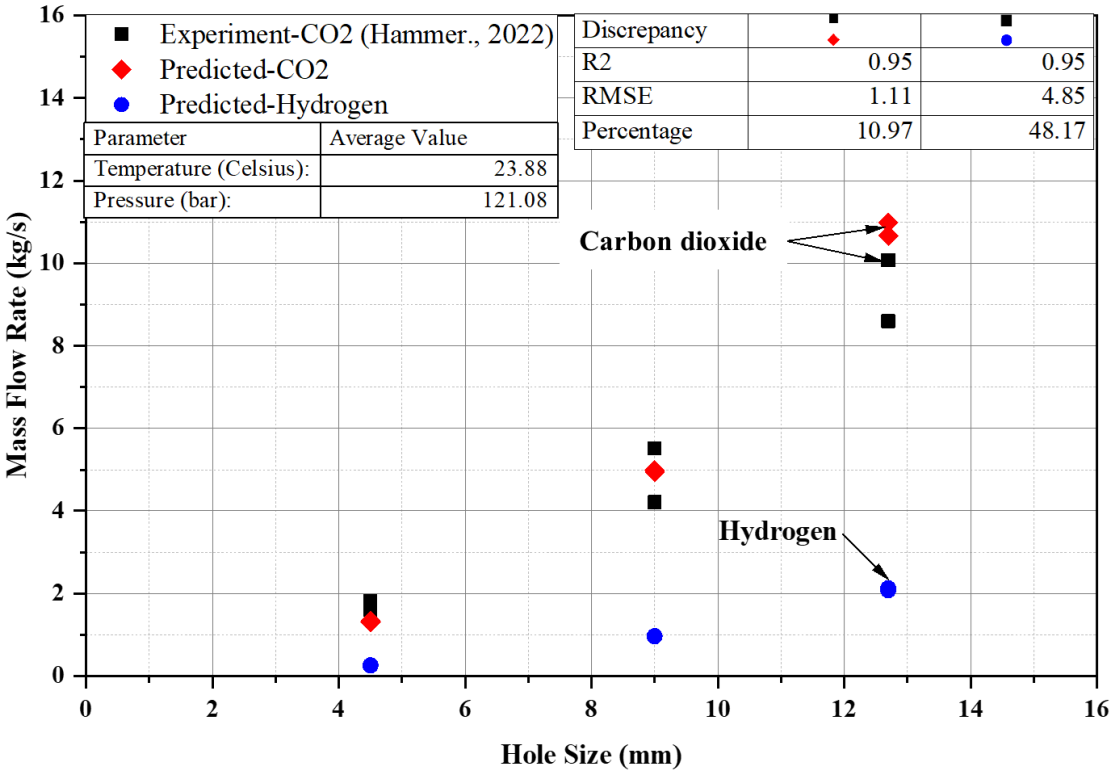

Figure 4. Comparison of experiment and predicted mass flow rates considering both CO_2 and Hydrogen gases

Table 4. Tabulation of mass flow rates

Test no.	*d* (mm)	P_0 (MPa)	CO_2-Experiment	CO_2-Predicted	Hydrogen-Predicted
13	12.70	12.77	8.59	8.15	1.79
16	4.50	12.17	1.60	3.43	0.75
17	4.50	12.40	1.81	3.70	0.81
18	12.70	12.41	10.07	8.82	1.94
20	9.00	11.40	5.52	6.21	1.37
21	9.00	11.50	4.21	5.39	1.19

4.2 Validation of Gas Flow from Tank Venting

A validation of gas flow during venting, considering pressure blowdown, was conducted based on an experiment from the Karlsruhe Institute of Technology (KIT). In this experiment, helium gas was stored in a pressurized tank connected to a release nozzle with a diameter of 1.0 mm. Before the test began, the

helium gas was allowed to cool to room temperature, reaching 293.15 K (20°C). Table 5 shows the parameters included in the test [1].

Table 5. Relevant parameters from the test as an input for pressure blow down estimation [1]

Parameter (Unit)	Value
Nozzle diameter (mm)	1.00
Gas temperature (K)	293.15
Reservoir pressure (MPa)	70.00
Internal volume of tank (L)	19.00
Discharge coefficient of nozzle	0.95
Release duration (s)	300.00
Heat capacity ratio of helium	1.40

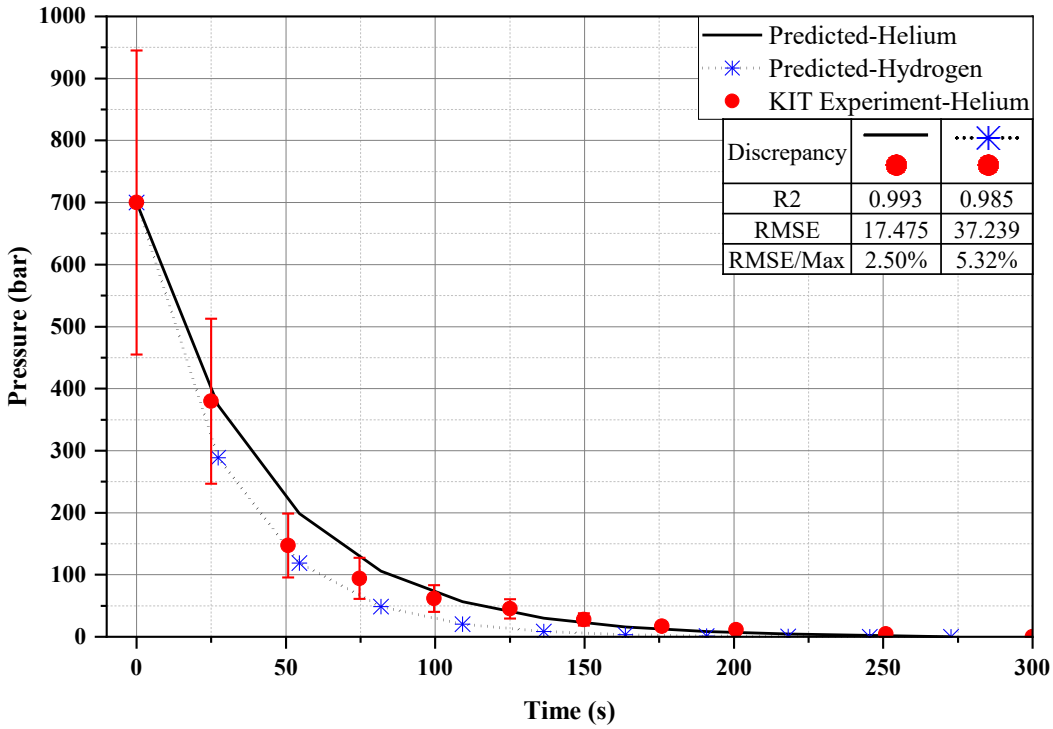

Figure 5. Comparison of experiment and predicted blow down profile considering both Helium and Hydrogen gases

Based on Equation (19), the pressure blowdown can be estimated and compared with the results of the KIT test. Figure 5 shows the comparison between the experimental blowdown profile and the predicted one. Since the method for estimating the mass flow rate is the same as in Equation (5), the

blowdown profile is sufficient for this validation. Additionally, hydrogen was included in this validation, considering experimental parameters with adjustments to molar weight and heat capacity ratio.

The validation results show good agreement, with only a 2.50 % discrepancy between the experimental and predicted blowdown for helium, and the data pattern aligns well, achieving an R^2 score of 0.993. For hydrogen, the comparison also shows a slight discrepancy of 5.32 %. This is due to the similar molar weights and heat capacity ratios of hydrogen and helium, which influence the same shape of the blowdown profiles.

5. CFD MODEL OF INCOMPLETE COMBUSTION

5.1 Brief Introduction of CFD Method

CFD method calculates both reacting and non-reacting flows by integrating conservation equations of momentum, mass, and energy. Mostly, CFD codes have several sub-models that account for turbulence, specie transport with reaction, radiation, or multiphase which are essential to develop a combustion model [19,37–39]. First, momentum, mass, and energy conservation can be written as follows [38]:

$$\frac{\partial}{\partial t}\left(\rho\bar{\upsilon}\right)+\nabla\left(\rho\bar{\upsilon}\bar{\upsilon}\right)=-\nabla p+\nabla\tau+\rho\bar{g} \quad (2$$

$$\frac{\partial\rho}{\partial t}+\nabla\left(\rho\bar{\upsilon}\right)=S_m \quad (2$$

$$\frac{\partial}{\partial t}\left(\rho h\right)+\nabla\left(\rho h\bar{\upsilon}\right)=\nabla q+\nabla\left(p\bar{\upsilon}\right)+\nabla\left(\tau\bar{\upsilon}\right)+S_h \quad (3$$

where ρ is fluid density (kg/m^3), υ is velocity component (m/s), τ is shear stress, g is gravitational acceleration which is 9.81 m/s^2, p denotes pressure (Pa), t denotes time (s), S_m is an additional mass source term (kg/m^3·s) (e.g., reacting particles such as coal). Subsequently, h denotes enthalpy (J), q represents heat flux per area (W/m^2) and S_h denotes volumetric heat source (W/m^3).

Real combustion problems typically involve turbulent flow. Therefore, a turbulence sub-model must be incorporated into the CFD model. In this case, the standard k-ε turbulence model was used. This model, first introduced by Launder and Spalding in 1974 [40], is widely adopted due to its robustness and lower computational cost compared to Direct Numerical Simulation (DNS) and Large Eddy Simulation (LES) [41,42]. By using two terms such as turbulent kinetic energy (k), and the dissipation rate (ε), the transport equations of k-ε turbulence model can be expressed as follows [38,40]:

$$\frac{\partial}{\partial t}(\rho k)+\frac{\partial}{\partial x_i}(\rho k \upsilon_i)=\frac{\partial}{\partial x_j}\left[\left(\mu+\frac{\mu_t}{\sigma_k}\right)\frac{\partial k}{\partial x_j}\right]+G_k+G_b-\rho\varepsilon+S_k \quad (31)$$

$$\frac{\partial}{\partial t}(\rho \varepsilon)+\frac{\partial}{\partial x_i}(\rho \varepsilon \upsilon_i)=\frac{\partial}{\partial x_j}\left[\left(\mu+\frac{\mu_t}{\sigma_\varepsilon}\right)\frac{\partial \varepsilon}{\partial x_j}\right]+C_1\frac{\varepsilon}{k}(G_k+C_3G_b)-C_2\rho\frac{\varepsilon^2}{k}+S_\varepsilon \quad (32)$$

where μ and μ_t denote fluid viscosity and turbulent viscosity (Pa.s), respectively. G_k and G_b are mean velocity gradient and buoyancy terms. Furthermore, C_1, C_2, C_3, σ_k, and σ_ε denote model constant which are 1.44, 1.92, 1.0, and 1.3, respectively. S_k and S_ε are source terms of both turbulent kinetic energy and dissipation.

A sub-model for non-premixed combustion was utilized in this study, as implemented in the ANSYS Fluent software. This modelling approach involves solving transport equations for one or two conserved scalars, known as mixture fractions, rather than solving separate equations for each chemical species [38]. The species concentrations are instead obtained from the calculated mixture fraction fields. Thermochemical properties are precomputed using a probability density function (PDF) and stored in a table for efficient lookup during the simulation [38]. The interaction between turbulence and chemical reactions is also modelled using the PDF. In this framework, non-premixed combustion is represented by incorporating the fuel-air mixture fraction, the specific heat of the mixture, and turbulent viscosity into the mass conservation equation. Consequently, the transport equation for the mixture fraction is expressed as:

$$\frac{\partial}{\partial t}\left(\rho \bar{f}\right)+\nabla\left(\rho \bar{\upsilon} \bar{f}\right)=\nabla\left(\left(\frac{\kappa}{c_p}+\frac{\mu_t}{\sigma_t}\right)\nabla \bar{f}\right)+S_m \quad (33)$$

where the fuel-air mixture fraction is denoted by f, κ denotes thermal conductivity of the mixture (W/m·K), c_p denotes specific heat capacity at constant pressure of the mixture (J/kg·K), μ_t is the turbulent viscosity (Pa.s), and σ_t denotes the Prandtl number. The turbulent viscosity can be described as follows which is related to turbulent kinetic energy and dissipation rate from k-ε turbulence model [40]:

$$\mu_t=C_\mu\rho\frac{k^2}{\varepsilon} \quad (34)$$

where C_μ is discharge coefficient which is 0.09 and ρ is fluid density (kg/m^3).

A chemical equilibrium assumption was applied in the model, where chemical reactions are assumed to occur instantly, eliminating the need for complex reaction kinetics and saving computational costs. Furthermore, in fuel-rich regions—where the equivalence ratio exceeds 1.5—combustion is considered extinguished, and unburned fuel coexists with the combustion products [38]. However, since the current

model assumes an instantaneous flame response, it is unable to capture the non-equilibrium effects such as ignition, extinction, and slow chemistry [38]. Therefore, it is suitable for the flaring case to measure the combustion efficiency [43].

5.2 INIG Field Test of Incomplete Combustion Quantification

The current validation of incomplete combustion was based on a flaring test conducted by Polish Oil and Gas Institute (INIG). A degassing flare manufactured by Esders was used in the test. Methane gas was employed, with a measured mass flow rate of 0.0012 kg/s at the diffuser outlet. According to the report, pure diffusion combustion occurred in the flare column, where fuel and air mixed within the combustion zone or immediately after ignition.

Field measurements were conducted using gas composition analysers and a hyperspectral camera. For gas analysis, the Horiba PG-350EU exhaust gas analyser was used to measure carbon monoxide (CO), carbon dioxide (CO_2), and oxygen (O_2). CO and CO_2 were measured using non-dispersive infrared absorption (NDIR) with a measurement range of 0 to 5000 ppm, while O_2 was measured using the paramagnetic method (PMA) within a range of 0 to 20%. Additionally, a Thermo FID TG flue gas analyser was used to measure unburned hydrocarbons in the flue gas region, approximately two meters from the centre of the flame.

Furthermore, an imaging Fourier Transform Infrared Spectroradiometer (FTIR) method was employed as the second quantification approach. This device which is Mini HC Telops detects methane destruction in the flare using a Fourier transform spectral analysis technique, which also enables the simultaneous identification and quantification of multiple gases in real time.

The results of the field test conducted by INIG show that the combustion efficiency of the methane flare ranged from 99.09% to 99.75% using the first method, and 99.77% was obtained using the second method. It can be concluded that both methods exhibit satisfactory consistency. The next section explains the procedure of the numerical analysis using the CFD method, and its resulting combustion efficiency will be compared with the test results.

5.3 CFD-based Incomplete Combustion Model

The CFD model was built with dimensions of 4.5 m × 1.8 m × 6.0 m for length, width, and height, respectively, defining the size of the fluid domain. The height of 6.0 m was considered sufficient to accommodate the flame path, as the measurement instrument in the field test was installed approximately 2.0 m above the flame centre.

The simulation was conducted using ANSYS Fluent, employing the standard k-ε turbulence model. The non-premixed combustion sub-model was used to calculate the chemical equilibrium of the combustion

process, with data for the fuel (CH_4), oxidizer (O_2), and other gas properties obtained from the Fluent database [38].

The bottom surface of the domain was treated as a wall boundary condition with a no-slip condition applied. The diffuser outlet face was defined as a mass flow inlet, where the gas enters the domain, while pressure outlet boundary conditions were applied to the remaining surfaces. Furthermore, the initial conditions in the domain were set to represent atmospheric air, with a gas composition of 76.7% N_2 and 23.3% O_2. The initial pressure throughout the domain was set at 1.01325 barg.

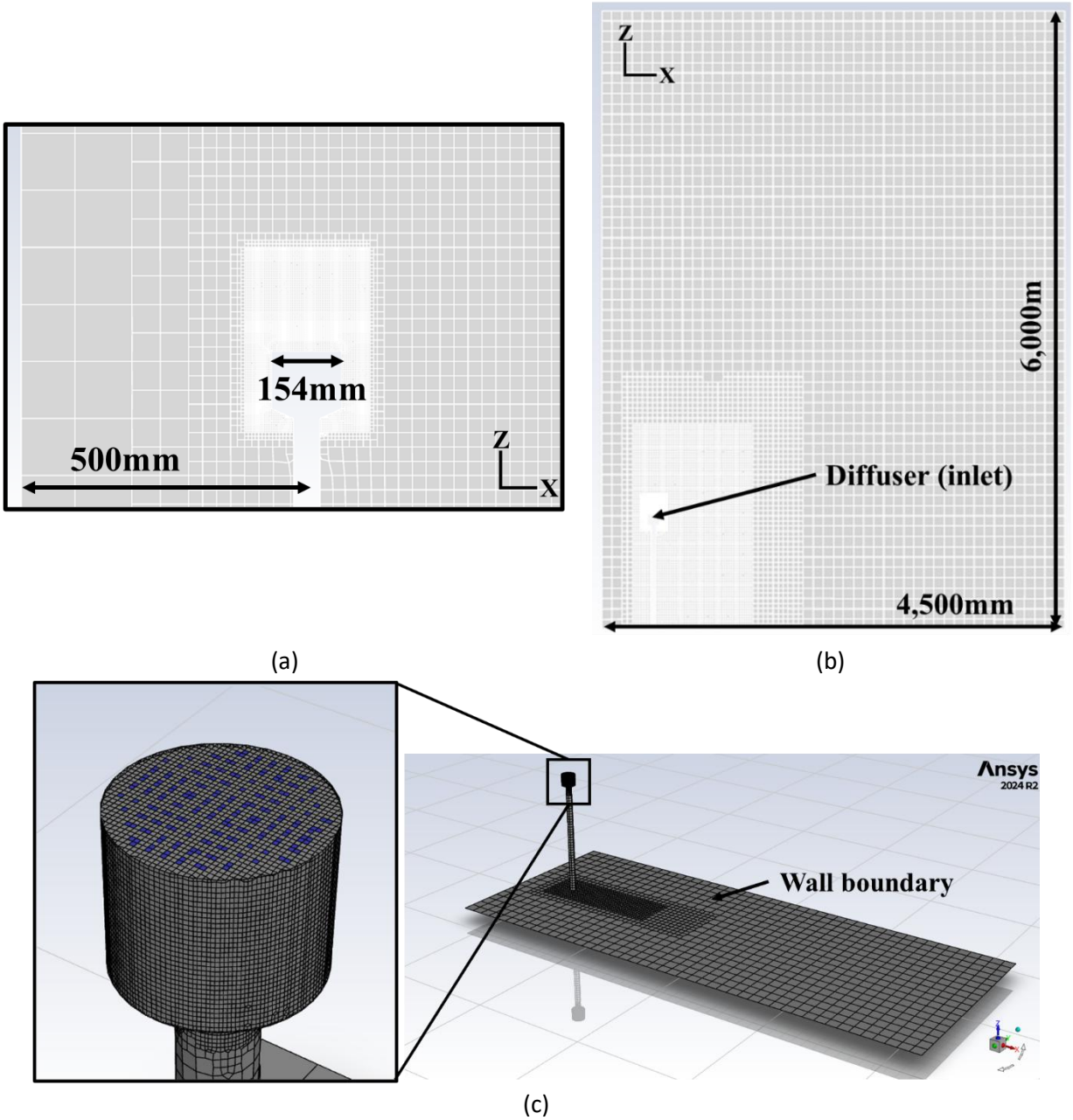

Figure 6. Cross-section and dimensions of the fluid domain (a, b) and the wall boundary face (c)

The mesh was configured with a minimum cell size of 3.0 mm and a maximum of 98.0 mm. Unstructured-hexahedral mesh configuration was used for the current model which hexahedral shape exhibit a superior accuracy compared with tetrahedral mesh. Subsequently, the finest mesh region was located near the inlet face to capture the small hole dimensions of the diffuser cassette. In total 621,999 cells were generated using this mesh configuration. Figure 6 shows a section of the entire fluid domain and highlights the wall boundary face used in the CFD analysis.

A steady-state approach was applied to the model to simplify the simulation while remaining suitable for flaring scenarios, as supported by a past study [43]. A coupled pressure–velocity scheme was used, along with second-order spatial discretisation. Additionally, the least-squares cell-based method was applied for gradient discretisation. The calculations were considered converged after 1,000 iterations.

5.4 Result of CFD Analysis

By considering the residual CH_4 mass fraction at the entire domain and compared with the mass fraction at the inlet, the combustion efficiency can be calculated based on Equation (25) [35]. In this case, the aim is to calculate how much CH_4 that burned during the flaring process in a percentage based on the field test result. Thus, the formulation can be modified as follows:

$$\eta_{burned} = 1 - \frac{\int_A \rho \upsilon Y_{fuel} dA}{\int_A \rho \upsilon Y_{fuel} dA_{inlet}} \times 100 = 1 - \frac{\dot{m}_{H_2,domain}}{\dot{m}_{H_2,inlet}} \times 100 \quad (35)$$

To improve accuracy, both volume and surface integral techniques provided in ANSYS Fluent were used to calculate the weighted average of mass flow rates in the entire fluid domain which represents the unburned fuel and at the inlet face, respectively. Since the inlet is represented by faces, surface integral technique could be used to calculate the weighted average. Table 6 presents the weighted average values obtained from both the internal fluid domain and the inlet face. By applying Equation (35), the combustion efficiency based on the mass flow rate of CH_4 from the CFD analysis was calculated to be as high as 99.998%. This value is still in good agreement with the combustion efficiency values obtained by the field test.

Table 6. Weighted-average values of CH_4 incomplete combustion analysis

Parameter	Fluid domain	Inlet face
Density (kg/m^3)	1.16	0.67
Velocity magnitude (m/s)	0.48	0.95
CH_4 mass fraction (kg/kg)	1.20×10^{-5}	0.91

Area (m^2)	1.67×10^{-3}	1.84×10^{-3}
CH_4 mass flow rate (kg/s)	1.13×10^{-8}	1.06×10^{-3}
Combustion efficiency (%)	**99.9986%**	

In addition, Figure 7 shows the contours of flame temperature and the mass fraction of H_2O produced by the combustion process. The maximum flame temperature reaches up to 1,440 K (1,166.85°C). At the threshold of visible flame, which is 798 K (525°C), the flame height extends approximately 1.23 m from the diffuser outlet.

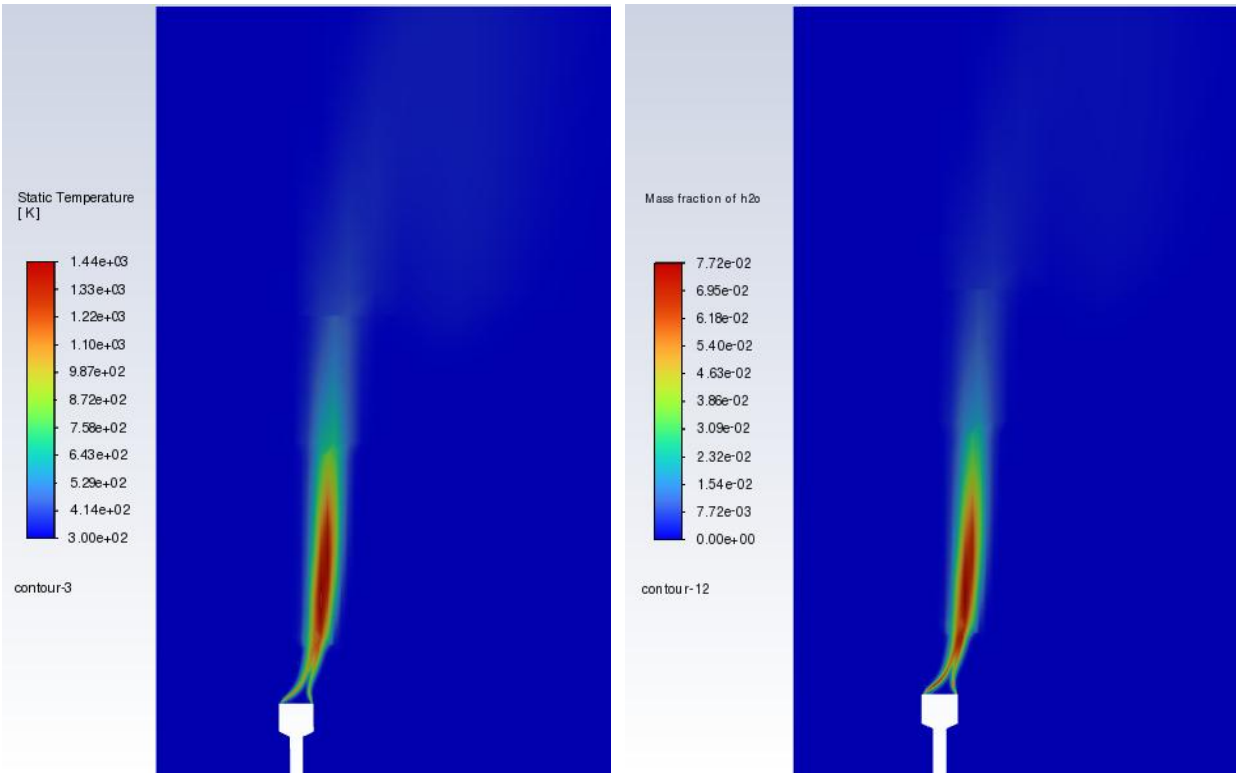

(a) (b)

Figure 7. Contours of flame temperature (a) and mass fraction of H_2O (b)

The same procedure was also performed for hydrogen flaring using the CFD method to compare the incomplete combustion with that of the methane flare. In this case, the main fuel was substituted to hydrogen (H_2) with a mass fraction of 1.0 kg/kg at the inlet. Furthermore, the PDF was updated to exclude the methane combustion mechanism, thus, the combustion products would consist only of H_2O Additionally, the mass flow rate at the inlet was set in the same manner as in the methane combustion case, which is 0.0012 kg/s. Table 7 shows the weighted average values resulting from the hydrogen flare case.

Table 7. Weighted-average values of H_2 incomplete combustion analysis

Parameter	Fluid domain	Inlet face
Density (kg/m^3)	1.15	0.08
Velocity magnitude (m/s)	0.59	7.75
H_2 mass fraction (kg/kg)	1.97×10^{-5}	1.00
Area (m^2)	1.67×10^{-3}	1.84×10^{-3}
H_2 mass flow rate (kg/s)	2.24×10^{-8}	1.06×10^{-3}
Combustion efficiency (%)	**99.9978%**	

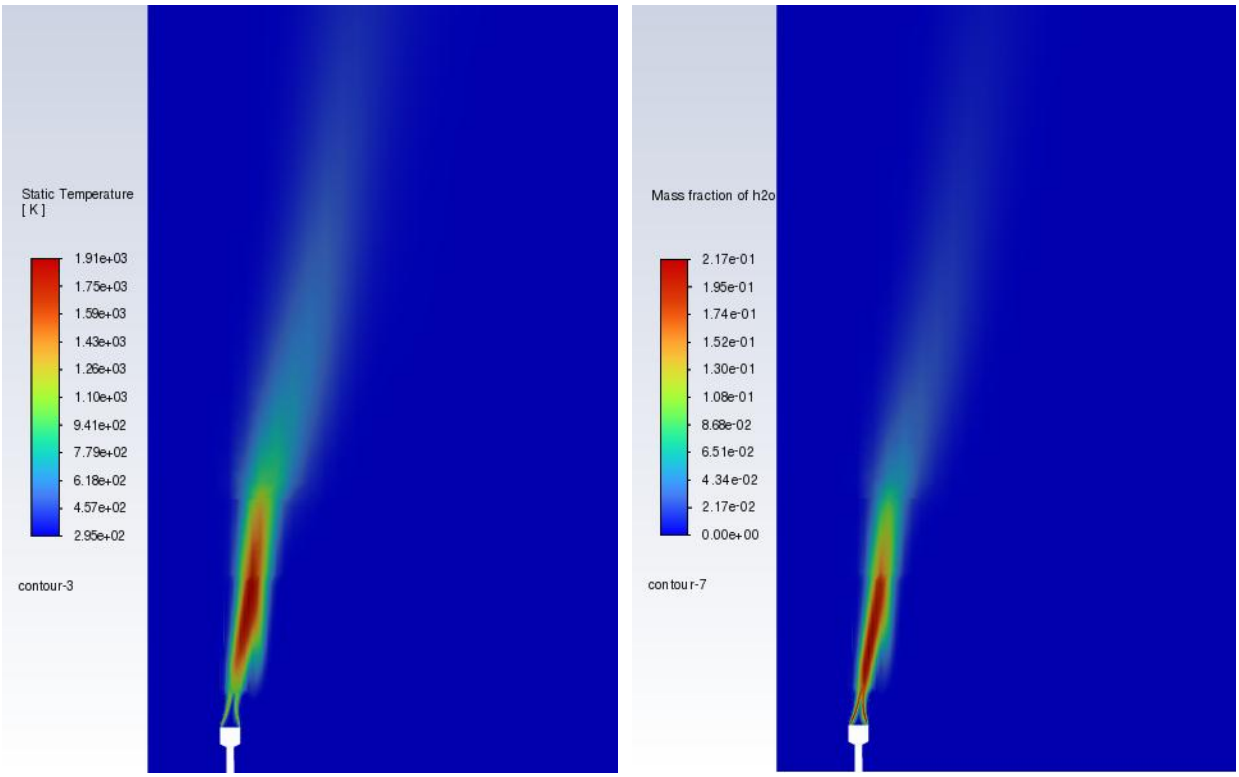

(a) (b)

Figure 8. Contours of flame temperature (a) and mass fraction of H_2O (b)

Under ideal conditions, both flare cases have high combustion efficiency of 99%, which aligns the field test results. Figure 8 shows the flame temperature and H_2O mass fraction from the hydrogen flare case. Compared to the methane flare, the hydrogen flare produces more water, with a maximum mass fraction of 0.217 kg/kg, while methane produces 0.077 kg/kg consider the same mass flow rate. Thus, the hydrogen flare produces almost three times more water than the methane flare. Overall, the total of unburned mass flow rate of both methane and hydrogen are 1.13×10^{-8} and 2.24×10^{-8} kg/s, respectively.

6. IN-HOUSE TOOL FOR CALCULATING HYDROGEN EMISSION

A predictive tool with a user-friendly front end was developed to estimate the total mass of hydrogen released from pipe joints and tank venting. The tool is designed to accelerate the calculation process and ensure ease of use. Currently, it accounts for emissions from pipe joints and tank venting. Further development may be required to incorporate additional emission sources. Figure 9 shows the main graphic user interface of the tool.

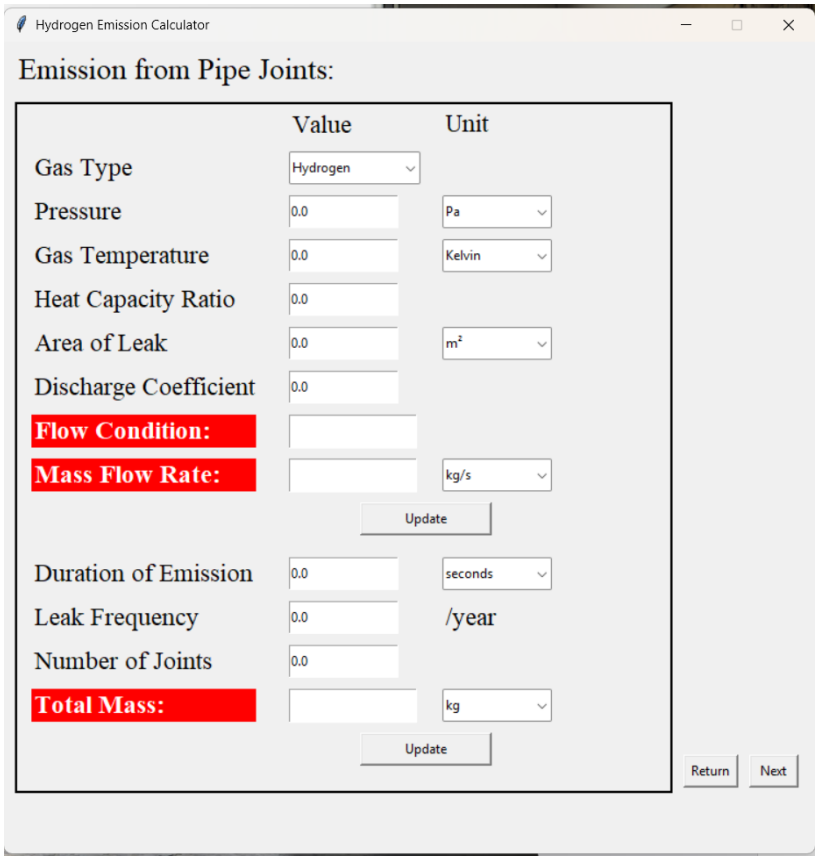

Figure 9. First page of interface for emission from pipe joints

The in-house tool was developed using Python and incorporates several key modules: *NumPy* for mathematical operations, *Pandas* for data handling—particularly with CSV files—and *Matplotlib* for data visualization and graph generation [44–46]. The tool features a graphical user interface (GUI) built with *Tkinter*, which is based on the *Tk* widget framework [47]. To enhance usability and simplify distribution,

the Python script was compiled into a single executable file (*.exe*) using *PyInstaller*, allowing the tool to be installed and run without requiring a Python environment.

6.1 Emission from Pipe Joints

To calculate the emission factor, several parameter values need to be entered. For example, suppose hydrogen gas is emitted from a flange connection, with an upstream pressure of 5.5 bar, a gas temperature of -253°C, and a leak diameter of 49.9 mm or 0.00196 m^2. Additionally, the discharge coefficient is 0.95, and the heat capacity ratio of hydrogen is 1.41. Figure 10 shows the interface with these parameters. Units can be selected using combo boxes to ensure consistency. Once the inputs are entered, simply click the "Update" button below the mass flow rate entry box. The mass flow rate value and flow conditions will then be displayed.

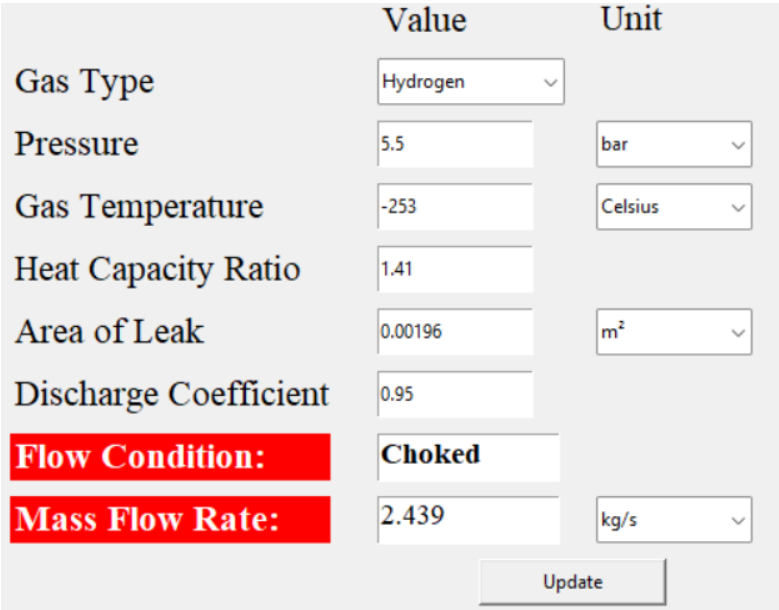

Figure 10. Interface for the emission factor with an example case

After obtaining the emission factor, the next step is to enter the parameters for the activity factor, as shown below. For example, the leak duration is set to 15 seconds, representing the emergency shutdown valve response time. Additionally, the leak frequency and number of flanges are both set to one. Then, click the "Update" button below the total mass label, and the result for the total mass will appear. Figure 11 shows the activity factor calculation.

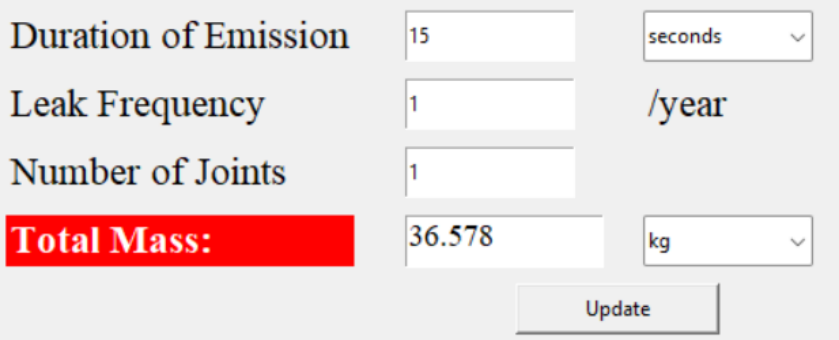

Figure 11. Interface for the activity factor with an example case

6.2 Emission from Tank Venting

For emissions from tank venting, the pressure drop should be considered, as it can impact the mass flow rate at any given time. In this scenario, a choked flow condition is assumed in the calculation, as most pressurised tanks have a reservoir pressure high enough to create a choked effect. Figure 12 shows the interface of the "Emission from Tank Venting" model.

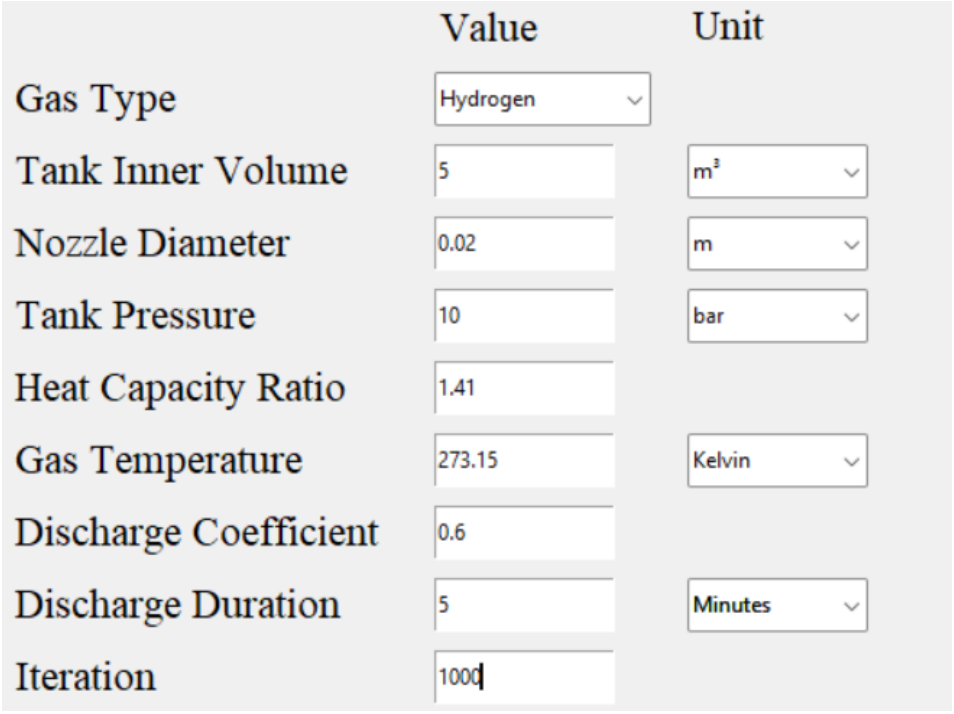

Figure 12. Interface for the emission factor from tank venting

In this example, a pressurised tank has an internal volume of 5.0 m^3. It stores and compresses hydrogen gas at a pressure of 10.0 bar and a temperature of 273.15 K. The nozzle diameter of the vent is 0.02 m (20 mm), with a discharge coefficient of 0.6. The venting time is set to 5.0 minutes to approximate the time

until the tank is drained. Please note that this venting time is an estimate rather than an exact duration until full drainage.

Iterations should be used to ensure smooth results, as this affects the area-under-the-curve calculation for discharge. Results are more accurate if the time step of the discharge duration is below 1.0 seconds. For example, if the discharge duration is 5.0 minutes, or 300 seconds, and it can be set 1,000 iterations, dividing 300 by 1,000 yields a time step of 0.3 seconds, which is well below the 1.0-second threshold. To get plots of pressure drop and mass flow rate, “Plot” button must be clicked and a pop up will appear. Figure 13 exhibits both pressure drop and mass flow rate plots.

(a)

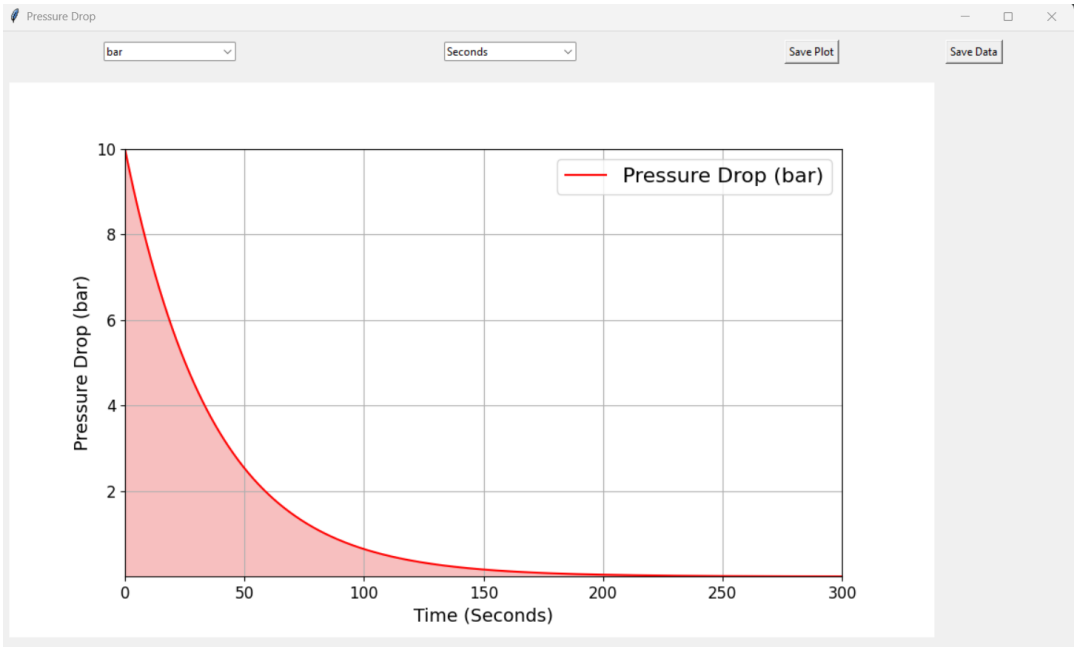

(b)

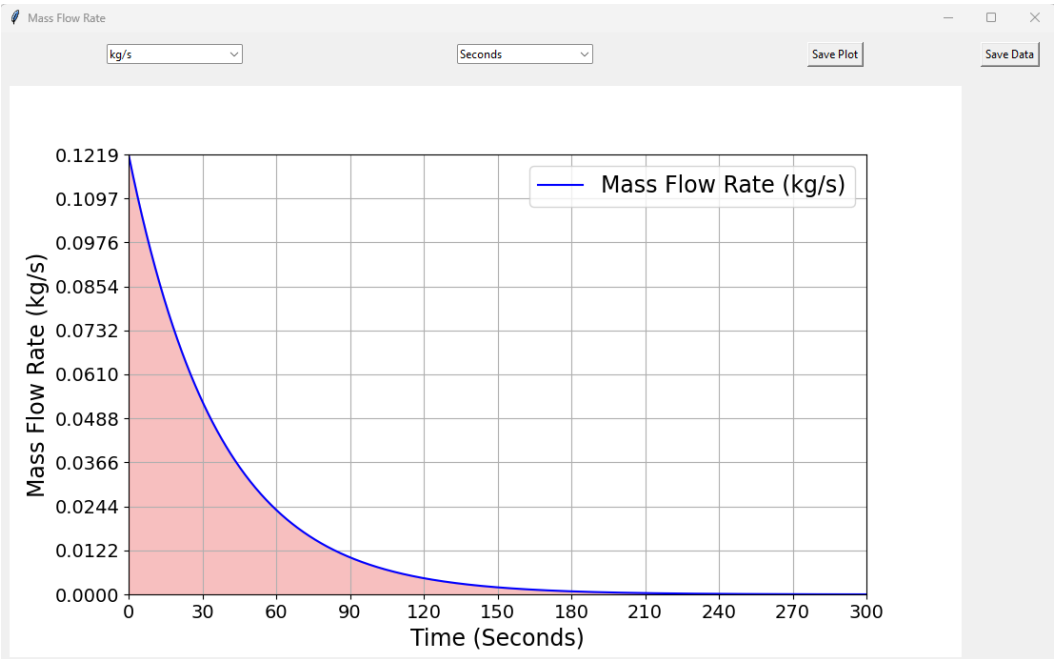

(c)

Figure 13. “Plot” buttons (a), pressure drop plot (b), and mass flow rate plot (c)

This program interface includes a feature to save both the plot image and data table. The “Save” buttons in the pop-up window allow you to save these files to the current directory. The plot image is saved in PNG format, while the data table is saved as a CSV file.

To account for the activity factor, a field is provided to enter the frequency value (per year). Figure 14 shows this input field and the resulting display of the total emitted mass, available in both kilograms and pounds. To display the result, click the “Update” button located at the bottom.

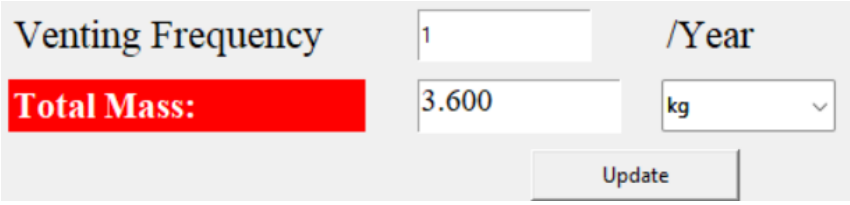

Figure 14. Field of activity factor for emission from tank venting

CONCLUSIONS

The general concept for hydrogen emission quantification—based on the deliverable D1.2 guideline and established methodology [16]—provides a structured approach for selecting suitable empirical correlations and numerical methods, such as CFD. These methods are applied to estimate the mass flow rate of hydrogen emissions from sources that cannot be directly measured. Emission sources are categorised as fugitive, vented along with additional of accidental release, incomplete combustion.

To ensure the reliability of both the empirical correlations and CFD model, several validation efforts were conducted. These involved comparing calculated results with available experimental data. Due to limitations in relevant experiments, only a few emission sources—such as pipe joints, tank venting, and incomplete combustion—were considered. Additionally, because of the scarcity of hydrogen-related experiments, validation was extended to studies involving other gases, such as carbon dioxide, helium, and methane. The validation results of selected emission sources showed good agreement, with discrepancies generally below 20% of the experimental data. To evaluate applicability to hydrogen, further calculations were performed using hydrogen gas, and the outcomes were compared against the validated results for other gases to assess the differences.

To improve usability and streamline the calculation process, an in-house tool was developed using Python. The tool features a graphical user interface (GUI) that simplifies input handling, including gas type selection and emission parameters. It includes modules for calculating emissions from pipe joints and tank venting, based on empirical correlations.

For tank venting scenarios, the tool also generates pressure blowdown and mass flow rate profiles over time, which can be visualised through graphs and exported as CSV files. These outputs are particularly useful for advanced analyses, such as CFD simulations involving time-dependent mass flow inputs.

However, the current study is limited in scope and does not cover all possible emission sources due to the lack of available data. Further surveys, detailed identification of emission types, and comprehensive literature reviews are needed to expand the database and improve the accuracy of hydrogen emission quantification for sources where calculation methods are applied.

REFERENCES

1. Dadashzadeh, M.; Makarov, D.; Molkov, V. Non-Adiabatic Blowdown Model: A Complimentary Tool for the Safety Design of Tank-TPRD System. In Proceedings of the International Conference on Hydrogen Safety, September 11-13, 2018, Hamburg, Germany; Semantic Scholar, 2017; pp. 1–18.

2. Hammer, M.; Deng, H.; Austegard, A.; Log, A.M.; Munkejord, S.T. Experiments and Modelling of Choked Flow of CO2 in Orifices and Nozzles. *Int. J. Multiph. Flow* **2022**, *156*, 104201, doi:10.1016/j.ijmultiphaseflow.2022.104201.

3. Kumar, S.; Kwon, H.T.; Choi, K.H.; Lim, W.; Cho, J.H.; Tak, K.; Moon, I. LNG: An Eco-Friendly Cryogenic Fuel for Sustainable Development. *Appl. Energy* **2011**, *88*, 4264–4273, doi:10.1016/j.apenergy.2011.06.035.

4. Buhaug, Ø.; Corbett, J.J.; Endresen, O.; Eyring, V.; Faber, J.; Hanayama, S.; Lee, D.S.; Lindstad, H.; Markowska, A.Z.; Mjelde, A.; et al. *Second IMO GHG Study 2009*; London, 2009;

5. Fevre, C. Le *A Review of Demand Prospects for LNG as a Marine Transport Fuel*; The Oxford Institute for Energy Studies, 2018; ISBN 9781784671143.

6. Livaniou, S.; Chatzistelios, G.; Lyridis, D. V.; Bellos, E. LNG vs. MDO in Marine Fuel Emissions Tracking. *Sustain.* **2022**, *14*, 1–12, doi:10.3390/su14073860.

7. International Maritime Organization *Emission Control Areas (ECAs) Designated under MARPOL Annex VI*; 2020;

8. DNV *Energy Transition Outlook 2022*. Bærum 2021, p. 118.

9. DNV *Hydrogen Forecast to 2050 Energy Transition Outlook 2022*; Hovik, 2022;

10. Ocko, I.B.; Hamburg, S.P. Climate Consequences of Hydrogen Emissions. *Atmos. Chem. Phys.* **2022**, *22*, 9349–9368, doi:10.5194/acp-22-9349-2022.

11. Paulot, F.; Paynter, D.; Naik, V.; Malyshev, S.; Menzel, R.; Horowitz, L.W. Global Modeling of Hydrogen Using GFDL-AM4.1: Sensitivity of Soil Removal and Radiative Forcing. *Int. J. Hydrogen Energy* **2021**, *46*, 13446–13460, doi:10.1016/j.ijhydene.2021.01.088.

12. Moradi, R.; Groth, K.M. Hydrogen Storage and Delivery: Review of the State of the Art

Technologies and Risk and Reliability Analysis. *Int. J. Hydrogen Energy* **2019**, *44*, 12254–12269, doi:10.1016/j.ijhydene.2019.03.041.

13. Kovač, A.; Paranos, M.; Marciuš, D. Hydrogen in Energy Transition: A Review. *Int. J. Hydrogen Energy* **2021**, *46*, 10016–10035, doi:10.1016/j.ijhydene.2020.11.256.

14. Yatsenko, E.A.; Goltsman, B.M.; Novikov, Y. V.; Izvarin, A.I.; Rusakevich, I. V. Review on Modern Ways of Insulation of Reservoirs for Liquid Hydrogen Storage. *Int. J. Hydrogen Energy* **2022**, *47*, 41046–41054, doi:10.1016/j.ijhydene.2022.09.211.

15. Frazer-Nash *Fugitive Hydrogen Emissions in a Future Hydrogen Economy*; Leatherhead, 2022;

16. MarcoGaz *Assessment of Methane Emissions for Gas Transmission and Distribution System Operators*; Brussel, 2019;

17. LaChance, J.; Houf, W.; Fluer, L.; Middleton, B. *Analyses to Support Development of Risk-Informed Separation Distances for Hydrogen Codes and Standards.*; Albuquerque, NM, and Livermore, CA (United States), 2009;

18. IOGP *Risk Assessment Data Directory – Process Release Frequencies*; London, 2019;

19. Vembe, B.E.; Rian, K.E.; Holen, J.; Lilleheie, N.I.; Grimsmo, B. Kameleon FireEx 2000 Theory Manual. *ComputIT* 2001, 134.

20. NASA Mass Flow Chocking Available online: https://www.grc.nasa.gov/www/k-12/airplane/mflchk.html (accessed on 10 October 2024).

21. Zhu, J.; Pan, J.; Zhang, Y.; Li, Y.; Li, H.; Feng, H.; Chen, D.; Kou, Y.; Yang, R. Leakage and Diffusion Behavior of a Buried Pipeline of Hydrogen-Blended Natural Gas. *Int. J. Hydrogen Energy* **2023**, *48*, 11592–11610, doi:10.1016/j.ijhydene.2022.10.185.

22. Parvini, M.; Gharagouzlou, E. Gas Leakage Consequence Modeling for Buried Gas Pipelines. *J. Loss Prev. Process Ind.* **2015**, *37*, 110–118, doi:10.1016/j.jlp.2015.07.002.

23. Zamara, K. Permeability of Soil Explained Available online: https://www.tensarinternational.com/resources/articles/the-permeability-of-soils-explained.

24. H2 Tools Basic Hydrogen Properties Chart Available online: https://h2tools.org/basic-hydrogen-properties-chart (accessed on 14 October 2024).

25. Zhu, S.; Shi, X.; Yang, C.; Li, Y.; Li, H.; Yang, K.; Wei, X.; Bai, W.; Liu, X. Hydrogen Loss of Salt Cavern Hydrogen Storage. *Renew. Energy* **2023**, *218*, 119267, doi:10.1016/j.renene.2023.119267.

26. Abreu, J.F.; Costa, A.M.; Costa, P.V.M.; Miranda, A.C.O.; Zheng, Z.; Wang, P.; Goulart, M.B.R.; Bergsten, A.; Ebecken, N.F.F.; Bittencourt, C.H.; et al. Large-Scale Storage of Hydrogen in Salt Caverns for Carbon Footprint Reduction. *Int. J. Hydrogen Energy* **2023**, *48*, 14348–14362, doi:10.1016/j.ijhydene.2022.12.272.

27. Chen, H.; Zheng, J.; Xu, P.; Li, L.; Liu, Y.; Bie, H. Study on Real-Gas Equations of High Pressure Hydrogen. *Int. J. Hydrogen Energy* **2010**, *35*, 3100–3104, doi:10.1016/j.ijhydene.2009.08.029.

28. Blaylock, M.L.; Klebanoff, L.E. Hydrogen Gas Dispersion Studies for Hydrogen Fuel Cell Vessels I: Vent Mast Releases. *Int. J. Hydrogen Energy* **2022**, *47*, 21506–21516, doi:10.1016/j.ijhydene.2022.04.262.

29. Wheeler, D. Tank Blowdown Math Available online: https://www.et.byu.edu/~wheeler/Tank_Blowdown_Math.pdf (accessed on 10 October 2024).

30. EMSA *Guidance on LNG Bunkering to Port Authorities and Administrations*; Portugal, 2018;

31. Correa-Jullian, C.; Groth, K.M. Data Requirements for Improving the Quantitative Risk Assessment of Liquid Hydrogen Storage Systems. *Int. J. Hydrogen Energy* **2022**, *47*, 4222–4235, doi:10.1016/j.ijhydene.2021.10.266.

32. Rigas, F.; Sklavounos, S. Evaluation of Hazards Associated with Hydrogen Storage Facilities. *Int. J. Hydrogen Energy* **2005**, *30*, 1501–1510, doi:10.1016/j.ijhydene.2005.06.004.

33. Vílchez, J.A.; Espejo, V.; Casal, J. Generic Event Trees and Probabilities for the Release of Different Types of Hazardous Materials. *J. Loss Prev. Process Ind.* **2011**, *24*, 281–287, doi:10.1016/j.jlp.2011.01.005.

34. Gupta, H.N. *Fundamentals of Internal Combustion Engines*; Second Edi.; PHI Learning Private Ltd: Delhi, 2013; ISBN 9788120346802.

35. Li, C.; Chen, X.; Li, Y.; Musa, O.; Zhu, L. Numerical Investigation on the Performance of Scramjet Combustor with a Novel Strut Configuration. *Appl. Therm. Eng.* **2019**, *159*, 113894, doi:10.1016/j.applthermaleng.2019.113894.

36. Gerlinger, P.; Stoll, P.; Kindler, M.; Schneider, F.; Aigner, M. Numerical Investigation of Mixing

and Combustion Enhancement in Supersonic Combustors by Strut Induced Streamwise Vorticity. *Aerosp. Sci. Technol.* **2008**, *12*, 159–168, doi:10.1016/j.ast.2007.04.003.

37. Abg Shamsuddin, D.S.N.; Mohd Fekeri, A.F.; Muchtar, A.; Khan, F.; Khor, B.C.; Lim, B.H.; Rosli, M.I.; Takriff, M.S. Computational Fluid Dynamics Modelling Approaches of Gas Explosion in the Chemical Process Industry: A Review. *Process Saf. Environ. Prot.* **2023**, *170*, 112–138, doi:10.1016/j.psep.2022.11.090.

38. ANSYS ANSYS FLUENT 12.0 Theory Guide 2009.

39. OpenCFD OpenFOAM User's Guide 2023.

40. Launder, B.E.; Spalding, D.B. The Numerical Computation of Turbulent Flows. *Comput. Methods Appl. Mech. Eng.* **1974**, *3*, 269–289, doi:10.1016/0045-7825(74)90029-2.

41. Mekonnen, A.T. Modeling and Numerical Simulation of Gas Explosions for Industrial Safety Analyses, Norwegian University of Science and Technology, 2019.

42. Bærland, T. Release and Spreading of Dense Gases: Turbulence Modeling with Kameleon FireEx, Norwegian University of Science and Technology, 2011.

43. Wang, A.; Sadovnik, I.; Tao, C.; Chow, J.; Sui, L.; Bottino, G.; Venuturumilli, R.; Evans, P.; Newman, D.; Lowe, J.; et al. Computational Fluid Dynamics Simulation of Combustion Efficiency for Full-Size Upstream Flare Experiments. *Atmosphere (Basel).* **2024**, *15*, doi:10.3390/atmos15070800.

44. Numpy Numpy Documentation Available online: https://numpy.org/doc/stable/ (accessed on 24 June 2025).

45. Pandas Pandas User's Guide Available online: https://pandas.pydata.org/docs/user_guide/index.html (accessed on 24 June 2025).

46. Matplotlib Using Matplotlib Available online: https://matplotlib.org/stable/users/index (accessed on 24 June 2025).

47. tkinter Tkinter - Python Interface to Tcl/Tk Available online: https://docs.python.org/3/library/tkinter.html.

APPENDIX A: GENERIC FAILURE FREQUENCY

The challenge lies in determining release frequency, which is typically linked to leak size and equipment type. However, hydrogen release frequency data is limited due to scarcity. To improve results, new or adjusted data is needed. The HyRAM project addresses this by using generic release frequencies from various databases and developing a Bayesian model to predict leak probabilities in hydrogen infrastructure components [17]. This model, based on offshore oil industry leakage data, calculates the means and standard deviations of leak rates for each component, which are then used to set the prior distribution parameters as initial estimates. Furthermore, Table 8 shows the distribution of equipment release frequency based on the result of Bayesian model. Furthermore, the mean of log-normal distribution can be used to obtain the release frequency, which is expressed as follows,

$$f_{release} = \exp\left(\mu + \frac{\sigma^2}{2}\right) \tag{36}$$

to obtain the variance of release frequency, it can be expressed as follows,

$$Var = \left[\exp\left(\sigma^2\right) - 1\right]\exp\left(2\mu + \sigma^2\right) \tag{37}$$

since there is a release size in the database, it defines as the percentage of leak area ($A_{\%}$) from the total cross-section area where the fluid is flown. For example, if the cross-section area of pipe is 100 cm^2, the 10% of release size of it should be 10 cm^2 or 3.56 cm of diameter. Thus, it can be expressed as follows:

$$A_{\%} = \frac{A_{leak}}{A_{pipe}} \times 100 = \frac{\sqrt{\frac{4d_{leak}}{\pi}}}{\sqrt{\frac{4d_{pipe}}{\pi}}} \times 100 \tag{38}$$

where A_{leak} and d_{leak} are area and diameter of the leakage, and A_{pipe} and d_{pipe} are area and diameter of the pipe cross-section, respectively.

Table 8. Distribution of release frequency

Component	Release size	μ	σ
Compressors	0.01%	-1.72	0.21
	0.10%	-3.92	0.48
	1%	-5.14	0.79
	10%	-8.84	0.84
	100%	-11.34	1.37
Cylinders	0.01%	-13.84	0.62
	0.10%	-14.00	0.61
	1%	-14.40	0.62
	10%	-15.00	0.63
	100%	-15.60	0.67

Filters	0.01%	-5.25	1.98
	0.10%	-5.29	1.48
	1%	-5.34	1.48
	10%	-5.38	0.87
	100%	-5.43	0.95
Flanges	0.01%	-3.92	1.26
	0.10%	-6.12	1.28
	1%	-8.12	1.18
	10%	-8.33	1.40
	100%	-12.75	1.83
Hoses	0.01%	-6.81	0.27
	0.10%	-8.64	0.55
	1%	-8.77	0.54
	10%	-8.89	0.83
	100%	-9.86	0.85
Joints	0.01%	-9.57	0.16
	0.10%	-12.83	0.48
	1%	-11.87	0.48
	10%	-12.02	0.53
	100%	-12.15	0.57
Pipes	0.01%	-11.86	0.66
	0.10%	-13.12	0.58
	1%	-13.87	1.13
	10%	-14.58	1.16
	100%	-15.73	1.71
Valves	0.01%	-5.18	0.07
	0.10%	-7.27	0.40
	1%	-9.68	0.96
	10%	-9.88	0.84
	100%	-12.00	1.33
Instruments	0.01%	-7.32	0.68
	0.10%	-8.50	0.79
	1%	-9.06	0.90
	10%	-9.97	1.07
	100%	-10.20	1.48